3-D Green's Functions of Microstrip Separated Into Simpler Terms—Behavior, Mutual Interaction, and Formulas of the Terms

Y. Leonard Chow, *Member, IEEE,* and Wan C. Tang

***Abstract*—Green's functions of microstrip substrate are important for microwave integrated circuit (MIC) analyses. Much work has been done by many researchers with successes over the years in gaining greater insight and simplifications into this complicated problem. This paper continues this trend with further simplification by arriving at formulas with insight for the Green's functions, both scalar and vector. Each Green's function is separated into three terms, namely: the quasi-dynamic, leaky wave, and surface wave. Practical MIC circuits require low surface-wave loss. This means that the formulas are constructed for frequencies low enough that with only the fundamental TM_0 surface-wave mode propagating. Formulas of dominant terms are emphasized. The formulas are accurate, with estimated errors from 1% to 2%. An important behavior observed is that the surface wave rises rapidly with frequency, at the four power even at low frequencies.**

***Index Terms*—Green's function, leaky wave, microstrip, simulated image, surface wave.**

I. Introduction

THIS PAPER is a continuation of the simplification and insight gained over the years on the Green's functions of a microstrip substrate.

From the 1960's to the 1980's, one used lengthy numerical integration of Sommerfeld integrals, scalar and vector, for full-wave solution. Mosig had a good summary of the achievements up to 1989 [1]. For approximation, in 1968, Silvester [2] used the simple static images and resulted in a quasi-static solution. In 1978 and 1980, Chow *et al.* [3], [4] modified the images slightly and obtained the quasi-dynamic solution that succeeded in including dispersion at low frequencies. In 1989, Mosig [1] then proved the equivalence between the images and the Sommerfeld integral.

In 1986, Lindell [5] introduced the continuous complex image concept of multilayer media. In late 1980's, Fang *et al.* [6] simplified the concept and produced the discrete complex images. In the 1990's, Chow *et al.* dropped the term "discrete" and then continued to simplify and expand the "complex images," through a series of papers [7]–[11]. The simplification and expansion were then carried on by others. To select representative ones, we have chosen Mittra [12], Aksun [13], Chan [14], and Sarkar [15] with his pencil function method. By this time, the integration of the Sommerfeld integrals was no longer tedious and lengthy. The results are the spatial Green's functions required for the moment-method solution of a printed circuit.

The derivation of the integrand in the Sommerfeld integral remained tedious, especially for the multilayer media. The integrand is the spectral Green's functions and the Sommerfeld integral is the actual Fourier transform converting the spectral to the spatial. In 1999, Chow *et al.* [9] rewrote the spectral Green's functions in a product series of repetitive 2×2 matrices, and greatly reduced the tediousness.

The Green's functions, in the spectral or spatial domain, are obviously unique, but the intermediate set of complex images used for Fourier transforming is nonunique. The nonuniqueness means that we may actually fix the image locations, say, to first three or four of those of the static images, and still get the same spatial Green's functions with similar accuracy. This simplification was named the simulated images method [16], [17].

In summary, this paper presents formulas for both scalar and vector potential Green's functions on a grounded substrate of a single layer. Precisely, a vector-potential Green's function is a dyadic Green's function giving the vector potential, after forming a dot product with a current vector. The formulas include the surface wave TM_0 in the three-dimensional (3-D) Green's functions. The current flow is assumed to be horizontal for microwave circuits.

II. Descriptive View of the Theory

The derivation of formulas of the Green's functions is a little involved, therefore, it may be profitable for us to give a descriptive view of the theory.

The microstrip point sources of unit current and charge are shown in Fig. 1. Each 3-D Green's function, scalar or vector, can be separated into three terms, namely: 1) quasi-dynamic; 2) leaky; and 3) surface waves.

The quasi-dynamic term comes from the multiple images of the source. For the scalar potential, they come from the static reflection coefficients, between the air–dielectric interface and the ground plane for the electrostatic field and scalar potential. For the vector potential, since the dielectric does not reflect the magnetostatic field, there is only one image from the ground plane.

The static reflections at the air–dielectric interface gradually change to the dynamic ones after multiple reflections at nonzero

Manuscript received December 17, 1999; revised October 19, 2000. This work was supported by the City University of Hong Kong under a strategic grant and by the Research Grant Council of Hong Kong under a competitive earmarked research grant.

The authors are with the Department of Electronic Engineering, City University of Hong Kong, Hong Kong (e-mail: eeylchow@cityu.edu.hk).

Publisher Item Identifier S 0018-9480(01)06135-X.

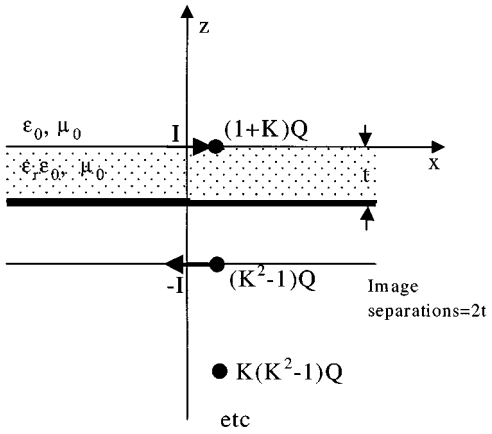

Fig. 1. Microstrip segment on a substrate. The quasi-dynamic images of the current I and one point charge Q of the segment are shown, for an observer in air. $K = (1-\varepsilon_r)/(1+\varepsilon_r)$. Quasi-dynamic images are static images used for calculation with the inclusion of distance phase delay.

frequencies, which are nonzero even for the vector potential. In the dynamic case, a part of the radiative power does not reflect, but leak, through the flat dielectric interface like the leakage in a Fabry–Perot resonator. These leaky reflections evidently give rise to the leaky-wave term.

The leakage is a function of the angle of the incident ray from the multiple images. The complexity of such a leakage effect can be greatly simplified by matching the complex or simulated images with the spectral Green's functions. For the leaky wave of the scalar Green's function, the simulated images are still simpler. The latter have only two dominant images: at the fixed quasi-dynamic image locations of the third and fourth. The corresponding images of the vector potential are just as simple, except that they are quite small and negligible.

For the scalar Green's function, the leaky wave provides the bulk of the radiation. For the vector Green's function, the quasi-dynamic term actually provides the bulk of its radiation.

Similar to the low leaky wave of the vector Green's function at low frequencies, the corresponding surface wave TE_1 is actually zero, below cutoff.

As shown in Figs. 13 and 14, each part of a Green's function has a different attenuation rate with distance along the substrate. For example at large distances ρ, the inductive quasi-dynamic field is that of a dipole and attenuates with $1/\rho^3$ on the substrate surface, the leaky wave being radiative, must attenuate with $1/\rho$, and the surface wave being a trapped wave must attenuate with $1/\sqrt{\rho}$. The different attenuation rates make the parts dominate in different distances, i.e., the quasi-dynamic at the near-field region, the leaky wave at the intermediate field region, and the surface wave at the far-field region.

Being radiative, both the leaky and surface wave must significantly rise with frequency, dielectric constant, and thickness of the substrate. The rise of these two inevitably "floods" over the inductive quasi-dynamic field and "pushes back" the boundaries of the three regions toward the source. The "floods" and "pushing backs" are pictorially observable in Fig. 13.

As observed later in (20), the rise in the surface wave is especially fast, proportional to the fourth power of frequency.

III. Theory—The Separation of the Spectral Green's Functions

A Green's function, scalar or vector, on the substrate surface in Fig. 1, has the form

$$G = G(\rho,\, t,\, \varepsilon_r,\, k_0) \tag{1}$$

where ρ is the distance from the source, in any horizontal direction because of circular symmetry. Next, t and ε_r are the thickness and dielectric constant of the grounded substrate. Finally, k_0 is the propagation constant in free space and is proportional to the operating frequency f. In view of this, without causing confusion, this paper simply calls k_0 the frequency.

The approach is to separate the spatial Green's functions of vector A and charge q into different terms. For each term, a formula can be synthesized. Following [7], and as shown in Fig. 1, the separations are

$$G_A^{xx} = G_{A0}^{xx} + G_{Af}^{xx} \tag{2a}$$

$$G_q = G_{q0} + G_{qf} + G_{q,\,\mathrm{sw}}. \tag{2b}$$

As indicated below (i.e., Section IV, and Table I, Figs. 8, 10, 12, and 14), at low frequencies, the leaky-wave term G_{Af}^{xx} is small. This means that the vector Green's function (2a) effectively has only the one dominant term, i.e., the quasi-dynamic G_{A0}^{xx}. The scalar Green's function in (2b), on the other hand, has all three terms dominant at different regions along the substrate surface.

One may note that the other vector Green's function G_A^{zx} is not included in (2a). G_A^{zx} is not of interest since a planar circuit normally does not have the z (vertical) direction lines.

Analytically, before the separation into terms, we have the Sommerfeld integrals

$$G_A^{xx} = \frac{\mu_0}{4\pi}\left[\frac{e^{-jk_0\rho}}{\rho} + \int_{-\infty}^{+\infty} \frac{1}{2jk_{z0}}\, R_{\mathrm{TE}}(k_\rho) \cdot e^{-jk_{z0}(z+z')} H_0^{(2)}(k_\rho\rho) k_\rho\, dk_\rho\right] \tag{3a}$$

$$G_q = \frac{1}{4\pi\varepsilon_0}\left[\frac{e^{-jk_0\rho}}{\rho} + \int_{-\infty}^{+\infty} \frac{1}{2jk_{z0}}[R_{\mathrm{TE}}(k_\rho) + R_q(k_\rho)] \cdot e^{-jk_{z0}(z+z')} H_0^{(2)}(k_\rho\rho) k_\rho\, dk_\rho\right]. \tag{3b}$$

On the substrate surface, $z = z' = 0$.

In each equation, the first term in the outer bracket is the source term. In the second term, the integrand is the spectral Green's functions. The latter are (4a) and (4b), shown at the bottom of the following page, and as shown in

$$r_{10}^{\mathrm{TE}} = \frac{k_{z1} - k_{z0}}{k_{z1} + k_{z0}}$$

$$r_{10}^{\mathrm{TM}} = \frac{k_{z1} - \varepsilon_r k_{z0}}{k_{z1} + \varepsilon_r k_{z0}} \tag{5}$$

$$k_{z0}^2 + k_\rho^2 = k_0^2$$

$$k_{z1}^2 + k_\rho^2 = \varepsilon_r k_0^2. \tag{6}$$

TABLE I
BEHAVIOR OF DIFFERENT FIELD TERMS ALONG SUBSTRATE SURFACE (LOW FREQUENCIES)

	Near field - inductive - quasi-dynamic	**Intermediate field***	**Far field***
Distance dependence	$1/\rho \to 1/\rho^3$	$1/\rho^2 \to 1/\rho$	$1/\sqrt{\rho}$
Charge amplitude	$(1+K)Q$, just a little change with k_0. ($K = (1-\varepsilon_r)/(1+\varepsilon_r)$)	Eq. (16): ampl.$\propto k_0^2$ (leaky wave)	Eq. (20): ampl.$\propto \beta^4$. β vs. k_0: linear then knee-shape rise at point "A". (TM_0 surface wave)
Dipole (charge) amplitude	$2Qt/\varepsilon_r$ (dc) t: substrate thickness	N.A.	N.A.
Current amplitude	I	Quasi-dynamic (leaky wave negligible)	Quasi-dynamic (TE_1 surface wave not excited)
Dipole (current) amplitude	$2It$ (dc)	N.A.	N.A.

* Leaky and surface wave amplitudes of scalar Green's function rise with k_0, gradually "floods" the near field and moves the field boundaries towards source.

The desired separation is first done in the spectral Green's functions. That is for the vector and scalar Green's functions, respectively,

$$R_{\rm TE} = R_{\rm TE0} + F_A \tag{7a}$$

$$\left(R_{\rm TE} + R_q\right) = \left(R_{\rm TE0} + R_{q0}\right) + F_q + \frac{2\beta \mathrm{res}_q}{k_\rho^2 - \beta^2}\, j2k_{z0}e^{jk_{z0}z} \tag{7b}$$

where the first terms of (7a) and (7b), the quasi-dynamic, are

$$R_{\rm TE0} = -e^{-j2k_{z0}t} \tag{8a}$$

$$R_{q0} = \frac{K\left(1-e^{-j4k_{z0}t}\right)}{1-Ke^{-j2k_{z0}t}}. \tag{8b}$$

The third term in (7b) of the TM_0 surface wave pole is

$$\mathrm{res}_q = \left(-\frac{1}{j2k_{z0}}\frac{k_{z0}^2}{k_\rho^2}\right) \cdot \left.\frac{j\varepsilon_r k_{z0}t + (k_{z1}t)\tan(k_{z1}t)}{\dfrac{d}{dk_\rho}\left[j\varepsilon_r k_{z0}t - (k_{z1}t)\tan(k_{z1}t)\right]}\right|_{k_\rho=\beta} \tag{9}$$

where β is the pole location. Formulas for the pole location are possible with the synthetic asymptote technique.

With the quasi-dynamic and surface-wave terms separated, the leftover terms, F_A and F_q, respectively, are the leaky wave (Fabry–Perot) terms.

With the spectral Green's functions separated into terms, we shall now convert each term to the spatial form, i.e., a formula. This is done in different convenient ways without directly integrating (3a) and (3b). A formula has the advantage that one can check its validity comprehensively and easily without massive computation or close scrutiny of its derivation.

The vector Green's function is much different (i.e., simpler) in behaviors from the corresponding scalar Green's function. Therefore, the formulas are presented below in separate sections.

IV. VECTOR (POTENTIAL) GREEN'S FUNCTION

A. Near Field with Quasi-Dynamic Formula

The quasi-dynamic images give the first terms in (2a) and (2b). The vector potential (2a) on the substrate surface is obtained by substituting (8b) into (3a), resulting through the Som-

$$R_{\rm TE} = -\frac{r_{10}^{\rm TE} + e^{-j2k_{z1}t}}{1 + r_{10}^{\rm TE}e^{-j2k_{z1}t}} \tag{4a}$$

$$R_q = \frac{2k_{z0}^2(1-\varepsilon_r)\left(1-e^{-j4k_{z1}t}\right)}{\left(k_{z1}+k_{z0}\right)\left(k_{z1}+\varepsilon_r k_{z0}\right)\left(1+r_{10}^{\rm TE}e^{-j2k_{z1}t}\right)\left(1-r_{10}^{\rm TM}e^{-j2k_{z1}t}\right)} \tag{4b}$$

merfeld identity [7] in a current source term and one image term, i.e.,

$$G_{A0}^{xx} = \frac{\mu_0}{4\pi}\left(\frac{e^{-jk_0\rho}}{\rho} - \frac{e^{-jk_0 r_0'}}{r_0'}\right) \tag{10a}$$

where

$$r_0' = \sqrt{\rho^2 + (2t)^2}.$$

This is the quasi-dynamic formula of the vector Green's function. It is of interest to point out that the source and image form a current dipole of moment

$$p_I = 2It \tag{10b}$$

where $I = 1$ for the Green's function by definition. Assume now that the operating frequency is not quasi-dynamic, but near dc ($k_0 \to 0$). Then, along the surface at large distance ρ, (10a) becomes

$$G_{A0}^{xx} \Rightarrow \frac{\mu_0}{4\pi}\left(\frac{p_I t}{\rho^3}\right). \tag{10c}$$

Fig. 2(a) shows the behavior of the separated quasi-dynamic field term for the vector potential with distance at two different frequencies. In Fig. 2(a), as well as Fig. 2(b), normalized frequency b of Mosig [1], where $b = \sqrt{\varepsilon_r - 1}(k_0 t)$, is used. The reason is that b is a gauge on the strength of the undesired surface wave, as discussed at the conclusion of Section V-C and the start of Section VI, where it states that one should have $b < 0.7$ and preferably much smaller.

To illustrate (10c), Fig. 2(a) puts in two distant markers. They are at $\rho = 2t$ and $k_0\rho = 1$. Marker 1 ($\rho = 2t$) gives the limit of the inductive quasi-dynamic term from a slope of $1/\rho$ to $1/\rho^3$ of (10c). Marker 2 ($k_0\rho = 1$) gives the limit that the field changes from inductive to radiative, as discussed in Section IV-B. The markers indicate shifts in the attenuation of the field along distances.

It may be useful later at (11a) to remember that, near dc, a current dipole has the same potential power dependence on ρ as a charge dipole with substrate $\varepsilon_r = 1$. The ρ dependence of the vector Green's function is observed in Fig. 2(a). To show its similarity, the corresponding scalar Green's function is observed in Fig. 2(b).

B. Intermediate and Far Field with the Quasi-Dynamic Formula

The quasi-dynamic term of (10a) is still the dominant term in the intermediate and far field away from dc, but at low frequencies before the appearance of the first TE_1 mode. The leaky wave appears, but is very small and can be neglected. The similarity in small and zero amplitude of the leaky and surface waves is expected, as the surface wave actually comes from the leaky wave.

The amplitudes of this leaky wave from F_A in (7a) have been obtained and plotted in Figs. 8, 10, 12, and 14. They are obtained in the same simplicity as the scalar F_q in (7b), which is discussed later in the section. However, the amplitude formula for the small leaky wave of the vector Green's function is not obtained.

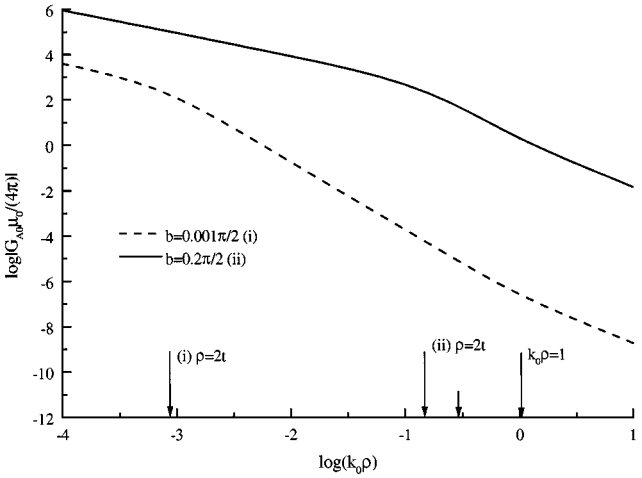

(a)

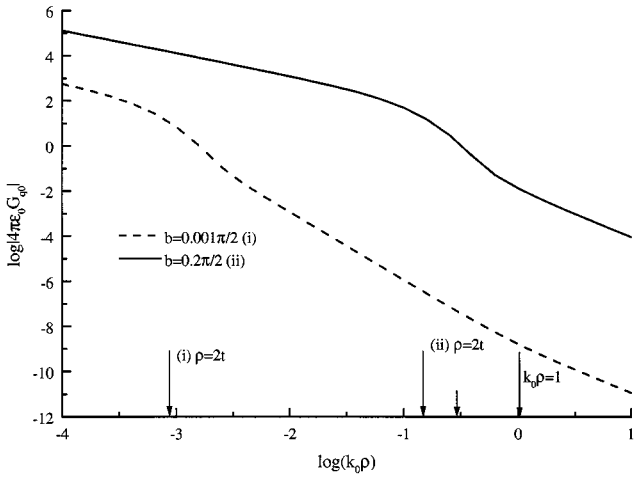

(b)

Fig. 2. Quasi-dynamic terms of the: (a) vector and (b) scalar Green's functions versus distance at different normalized frequencies ($b = \sqrt{\varepsilon_r - 1}k_0 t$). The markers $\rho = 2t$ and $k_0\rho = 1$ are given. The unlabeled marker is $\sqrt{\varepsilon_r}k_0\rho = 1$.

Due to the radiation at nonzero frequencies, at intermediate and far distances, the dominant quasi-dynamic term rises up from a dependence of ρ^{-3} at (10c) to reach ρ^{-2}, as shown in Figs. 2(a), 8, 10, 12, and 14.

V. Scalar (Potential) Green's Function

A. Near Field with Quasi-Dynamic Formula

The scalar Green's function is obtained by substituting (8b) into (3b), resulting through the Sommerfeld identity [7] in a charge source term and an infinite series of images, as shown in Fig. 1, and as follows:

$$G_{q0} = \frac{(1+K)}{4\pi\varepsilon_0\rho}\, e^{-jk_0\rho} + \sum_{i=1}^{\infty} \frac{K^{i-1}(K^2-1)}{4\pi\varepsilon_0 r_i}\, e^{-jk_0 r_i} \tag{11a}$$

where

$$K = (1-\varepsilon_r)/(1+\varepsilon_r)$$
$$r_i = \sqrt{\rho^2 + (2it)^2}, \qquad i = 1, 2, 3, \ldots.$$

The magnitudes of the charge images in the sum have been obtained from the classical image method [2]–[4].

The multiple charge images form dipole moments with the source. They can be summed through an integration of a geometrical series resulting in a total dipole moment of

$$p = 2Qt/\varepsilon_r. \tag{11b}$$

A comparison of this electric dipole moment and the magnetic one in (10b) indicates that this dipole moment is surprisingly much lower, divided by ε_r, the dielectric constant.

Fig. 2(b) has the same markers as Fig. 2(a). In the near field close to the source, it is clear that the Green's function attenuates as $1/\rho$, scalar or vector. With the phase exponentials included in (11a), the field is quasi-dynamic. In the far field of the quasi-dynamic term beyond marker 1, the vector Green's (potential) function has a field dependence of $1/\rho^3$ of (10c). It is interesting to point out the effect of ε_r on the corresponding scalar Green's function. Having been divided by ε_r in (11b), the $1/\rho^3$ field dependence of the small electric dipole only emerges from the low leaky and surface waves at very low frequencies, such as 20 MHz for a substrate of $t = 1$ mm. Also, beyond marker 2 at high ε_r, the long series of multiple images has long phase delays even in moderate frequencies; this reduces the dependence to $1/\rho^n$, where we may have $n \to 2$.

The dependence of the $1/\rho^3$ is difficult to observe directly in the total scalar Green's function in Figs. 7, 9, 11, and 13. As introduced at the conclusion of Section II, the reason is the leaky and surface waves normally "flood" over and obscure the relevant quasi-dynamic region. The "flooding" may move toward the source closer than marker 2 of $k_0\rho = 1$ at high frequency and high ε_r. This movement is understandable. As at marker 2, in the substrate, the phase is already $\sqrt{\varepsilon_r}k_0\rho = \sqrt{\varepsilon_r}$, larger than unity. When the phase there approaches unity, one expects the quasi-dynamic radiation becomes significant. This is even more so with leaky and surface wave because of their rapid rises with frequency, as discussed in later sections.

The indirect effect of the $1/\rho^3$ term of the scalar Green's function is readily observed. This term itself is small because of the division by ε_r in (11b). However, for high ε_r, the original $1/\rho$ dependence, close to the source, would have to make a sharp drop to reach the small $1/\rho^3$ term at the approximate distance of $\rho = t$ (the thickness of the substrate) from the source. This sharp drop appears as fast as $1/\rho^5$ and is readily observable in a scalar Green's function.

B. Leaky-Wave Formula

For the formulas of the leaky-wave region, we can rewrite (7b) as follows:

$$F_q = \left(R_{\mathrm{TE}} + R_q\right) - \left(R_{\mathrm{TE0}} + R_{q0}\right) - \frac{2\beta \mathrm{res}_q}{k_\rho^2 - \beta^2}\, j2k_{z0}e^{jk_{z0}z}. \tag{12}$$

With numerical experimenting, it is found that F_q can be approximated with only two simulated images at locations of the third and fourth (i.e., at distances of $4t$ and $6t$ below the source) of the quasi-dynamic images. That is, we can put

$$F_q = a_{q1}e^{-j4k_{z0}t} + a_{q2}e^{-j6k_{z0}t} \tag{13}$$

where the coefficients a_{qn} are to be found through matching (13) numerically at two data points, each in the spectral k_{z0} plane from (12).

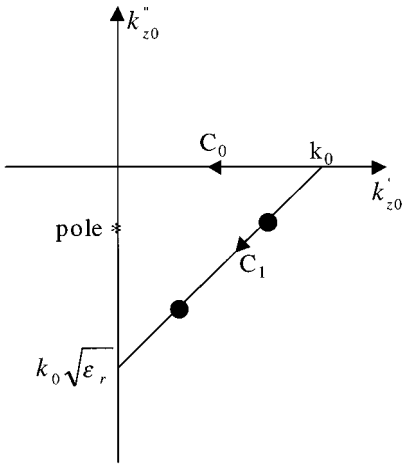

Fig. 3. Two data points along the C_1 path on the spectral plane of k_{z0}.

Following [7], as shown in Fig. 3, the two data points are chosen with the midpoint rule, along a straight path C_1 on the complex k_{z0} plane

$$C_1\colon k_{z0} = k_0\left[-jt_0 + \left(1 - \frac{t_0}{T_0}\right)\right], \qquad 0 \le t_0 \le T_0. \tag{14}$$

T_0 is taken as $\sqrt{\varepsilon_r}$ in this paper, thus, they are probably near the possible leaky-wave poles. With the accurate Green's functions obtained later in Figs. 7–14, it is a good choice. This implies the following. For the leaky-wave images, following the above procedure, it is not necessary to tediously locate the leaky-wave poles. Two somewhat nearby data points on the spectral plane in Fig. 3 are sufficient.

With the coefficients a_{qn} found, (13) can be substituted in (3b), through the Sommerfeld identity, we get

$$G_{qf} = \frac{1}{4\pi\varepsilon_0}\sum_{i=1}^{2} a_{qi}\frac{e^{-jk_0r_i'}}{r_i'} \tag{15}$$

where

$$r_i' = \sqrt{\rho^2 + \left[2(i+1)t\right]^2}, \qquad i = 1, 2.$$

It is interesting at this point to discuss the physical basis why only two leaky-wave images are needed and why they are located in the third and fourth image locations in Fig. 1. The leaky wave discussed in this paper is formed from multiple reflections in the substrate. A simple picture of the "rays" of the multiple reflection indicates that the number of reflections corresponds to the image number. With more reflections, the ray path is longer and the ray loses its static characteristics and acquires

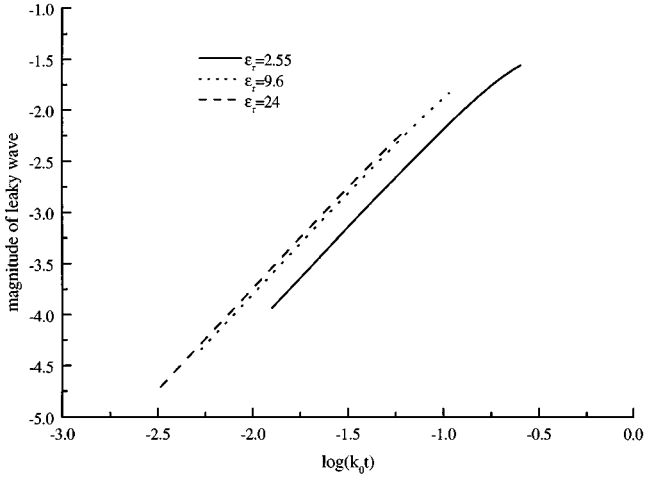

Fig. 4. Magnitudes of leaky wave (radiation) versus frequency in k_0.

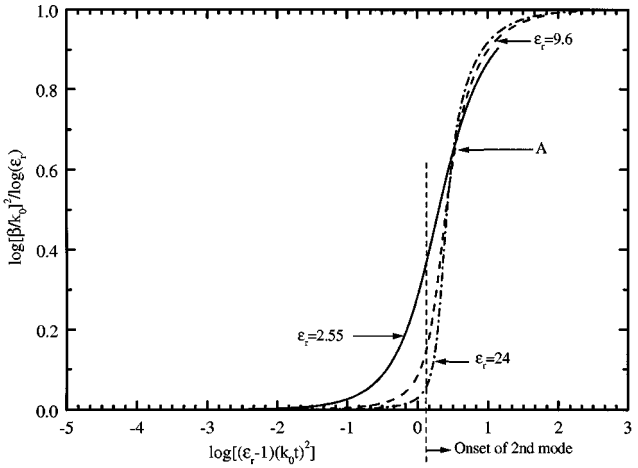

Fig. 5. log-log plot of the surface-wave pole with rearranged variables. The dielectric constants are 2.55, 9.6, and 24.

more wave characteristics. This is why the leaky-wave images are stronger at image locations of higher numbers of three and four. At even higher numbers, the leaky wave turns into a surface wave, but the surface wave has already been extracted.

The substrate thickness t is thin at the frequency of interest in this paper. This means that the phase delay between the two leaky wave images is small. Therefore, the amplitude of the (total) leaky wave can be estimated by simply adding the amplitudes of the two images. In this way, the change of leaky-wave amplitude is estimated with frequency, in terms of $k_0 t$ in Fig. 4, which shows that the amplitude of the leaky-wave radiation increases with the frequency.

Equations (12), (13), and (15) constitute the formula of the leaky wave. They are not too complicated, as they are, at the most, 2×2 matrices. Still, the four equations are not like one equation for insight. To gain more insight about the leaky-wave radiation, a numerically fitted equation on the absolute magnitude (without phase and unit) from Fig. 4 and (15) is given as follows:

$$\left|a_{q1} + a_{q2}\right| = \frac{\sqrt{\varepsilon_r - 1}}{2} (k_0 t)^2. \tag{16}$$

Evidently with a simple sum of two images, this amplitude formula cannot be very accurate compared with (15) plus (13) and (12). The average errors are 12% to 2%, respectively. Despite this, (16) does give an insight that the leaky-wave amplitude of the scalar Green's function is proportional to $(k_0 t)^2$. The square dependence is probably caused by the Fabry–Perot action. This is at low frequencies before the sharp rise of surface-wave power at point "A," as discussed in the following section.

C. Surface-Wave Formula

The original equations of surface wave pole location are three simultaneous transcendental equations given by (4b) and (6) or by [18]. By numerical means, one finds the pole location β for a given frequency in k_0 from the three equations.

Analytically, the three equations do not suggest any simple formulas for the pole location other than that there are two asymptotes, i.e., $\beta = k_0$ at low frequencies and $\beta = \sqrt{\varepsilon_r}\, k_0$ at high frequencies. With a little thought, the asymptotes suggest a rearranged surface-wave propagation y for β. Also, (6) suggests a rearranged free-space propagation x for k_0. Analytically, they are

$$y = \frac{2}{\log \varepsilon_r} \left(\log \frac{\beta t}{k_0 t} \right) \tag{17a}$$

$$x = \log \left[(\varepsilon_r - 1)(k_0)^2 \right]. \tag{17b}$$

With the rearranged variables, the β versus k_0 curve becomes as shown in Fig. 5. There, the asymptotes at low and high frequencies become simply two parallel lines at $y = 0$ and $y = 1$, independent of the dielectric constant ε_r. Due to the rearranged x, the dispersion with ε_r of the graphs at the intermediate frequencies in Fig. 5 is greatly reduced so that they actually cross approximately at point A with the x–y coordinates at (0.51, 0.633). The slope at the crossing point is a function of ε_r.

With the slope and point A found, we can now neglect the frequency beyond A. The reason is that the second surface-wave mode TE_1 begins to propagate, as shown in Fig. 5. We may consider the slope line passing through point A as a pseudo-asymptote.

This asymptote together with the low frequency asymptote may now form a synthetic asymptote through a hyperbola fit for the lower frequencies. The result is the following pole location formula of TM_0:

$$y\left[y - 0.633 - \frac{\sqrt{\varepsilon_r}}{2}(x - 0.51)\right] = 0.021. \tag{18}$$

The maximum error of the formula is 5% for $\varepsilon_r = 24$ at the maximum frequency point at A. The error is less at lower ε_r and at lower frequencies.

Equation (17b) can be written as $x = \log b^2$, and then b is the normalized frequency used by Mosig [1] in his plots of the Green's functions. At point A in Fig. 5, $b = 0.714$, which means that, beyond this value of b, the higher TE_1 start to propagate and the surface wave has become too large for low-loss microstrip circuits.

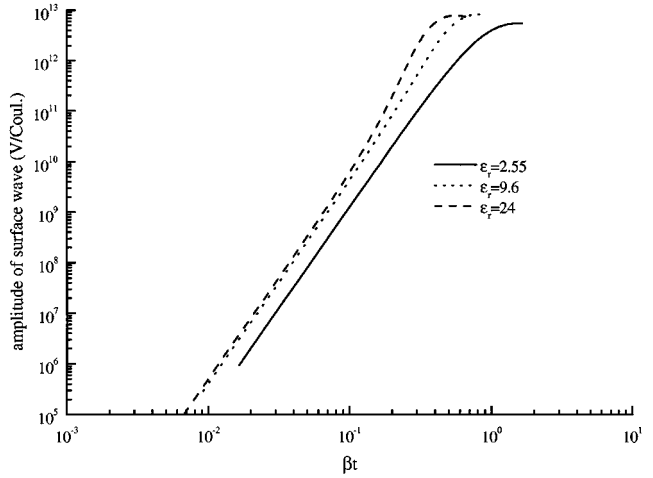

Fig. 6. Amplitude of the surface wave TM_0 versus frequency in k_0 for different ε_r. Amplitude volt per coulomb is not 1 F since the field point V and source point Q do not coincide.

After the surface-wave pole location is found, the residue res_q can be calculated easily from (9). With that, we get the spatial scalar Green's function of the surface-wave region by using the residue theorem, i.e.,

$$G_{q,\mathrm{sw}} = \frac{1}{4\pi\varepsilon_0}(-2\pi j)\mathrm{res}_q H_0^{(2)}(\beta\rho)\beta = \frac{-j\mathrm{res}_q}{2\varepsilon_0} H_0^{(2)}(\beta\rho)\beta \tag{19}$$

where res_q is defined in (9) and $\beta \cong k_0$ at low frequencies. At large distance ρ, the Hankel function of (19) indicates that the scalar Green's function is proportional to $1/\sqrt{\rho}$.

Equations (9) and (17)–(19) form the formula of the fundamental surface wave TM_0 of the scalar Green's function. With the definitions of (17), (18) directly gives the pole location β as a function of frequency k_0. With pole location, (9) gives the pole residue. With pole residue, (19) gives the surface-wave portion of the scalar Green's function.

Fig. 6 indicates that the log of amplitudes of the fundamental surface wave TM_0 of the scalar Green's function increases linearly with the log of βt at the fourth power. Its spread with ε_r is quite small. Fig. 5 indicates that, at the low frequencies concerned, the pole location β approaches the frequency k_0.

If Fig. 6 and (9) still provide insufficient physical insight, (9) can be replaced by the curve-fitted equation from Fig. 6. To substitute into (19), we then have the amplitude equation

$$\left|\frac{\mathrm{res}_q}{2\varepsilon_0}\beta\right| = \frac{1}{2}\left(\frac{\varepsilon_r - 1}{\varepsilon_r}\right)^3 \frac{1}{\varepsilon_0 t}(\beta t)^4. \tag{20}$$

The log-log plots in Fig. 6 are not exactly straight lines. This means that (20) obviously cannot be as accurate as the formula with (9), and (18), and (19) together. The average errors, respectively, are 9% and 3%. However, the above equation does give the insight that the surface-wave amplitude is proportional to β^4 and t^3. This β^4 ($\beta \approx k_0$) dependence of the surface wave, compared to the β^2 dependence of the leaky waves in (16), is what enables the surface wave to "flood over" the leaky wave at higher frequencies, such as that in Fig. 13. This rapid β^4 dependence also implies that the surface-wave amplitude can easily rise to an intolerable limit with a small rise in frequency.

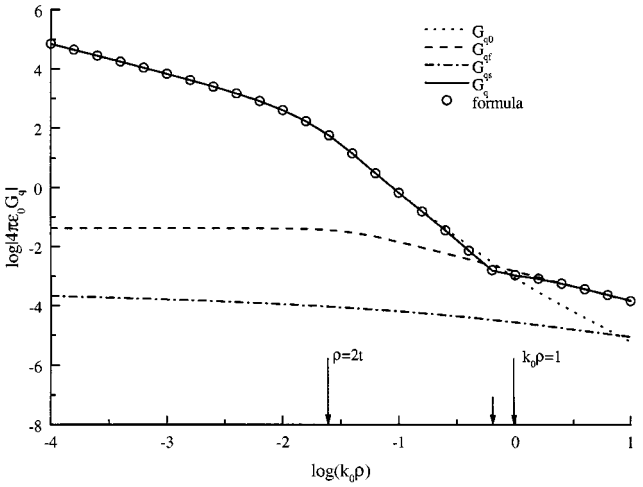

Fig. 7. Scalar Green's function for $\varepsilon_r = 2.55$, $b = 0.01\pi/2$. The dots are from the formulas. The rest of the continuous plots are from the complex image method. Markers 1 and 2 are at $\rho = 2t$ and $k_0\rho = 1$. The unlabeled marker is $\sqrt{\varepsilon_r}k_0\rho = 1$. Labels: G_{q0} = quasi-dynamic, G_{qf} = leaky wave (Fabry–Perot), G_{qs} = surface wave, G_q = sum.

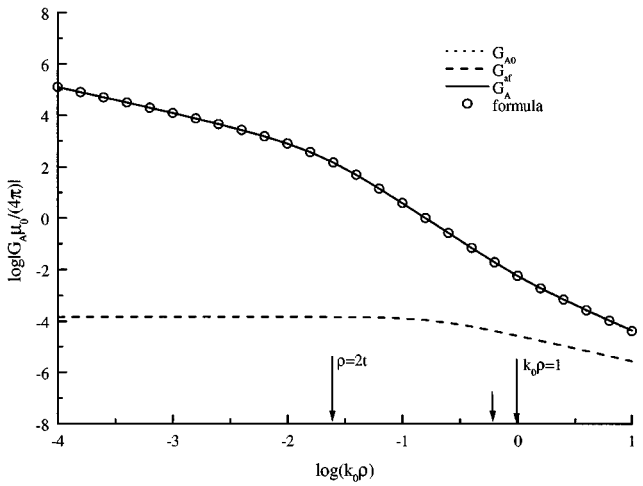

Fig. 8. Vector Green's function for $\varepsilon_r = 2.55$, $b = 0.01\pi/2$. Labels: G_{A0} = quasi-dynamic, G_{Af} = leaky wave (Fabry–Perot), G_A = sum.

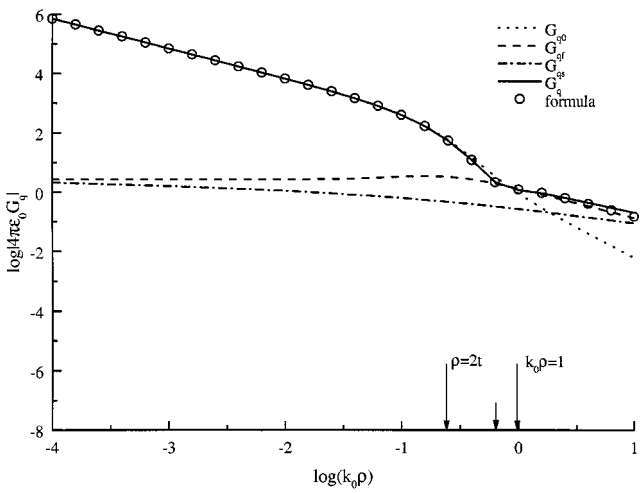

Fig. 9. Scalar Green's function for $\varepsilon_r = 2.55$, $b = 0.1\pi/2$.

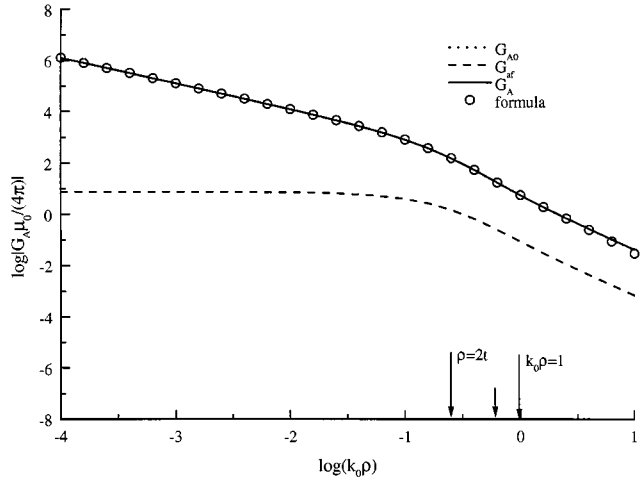

Fig. 10. Vector Green's function for $\varepsilon_r = 2.55$, $b = 0.1\pi/2$.

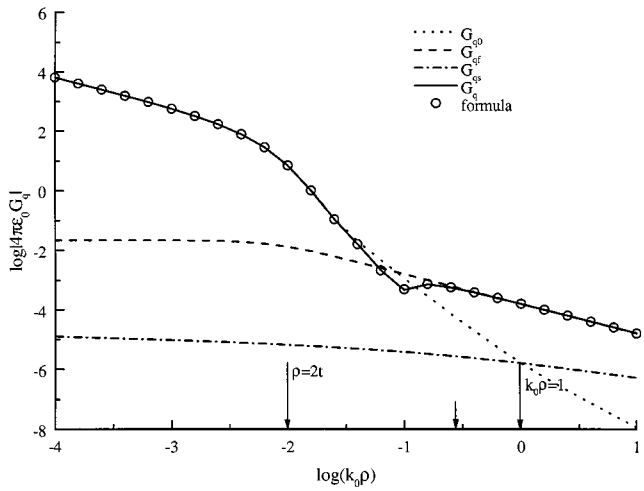

Fig. 11. Scalar Green's function for $\varepsilon_r = 12.9$, $b = 0.01\pi/2$.

VI. Contribution and Behavior of the Formulas to the Total Green's Functions

Each 3-D Green's function, scalar and vector, has been separated into three parts, namely. 1) quasi-dynamic; 2) leaky (Fabry–Perot); and 3) surface wave. For better illustration of their behaviors, in the figures of the Green's functions, each part is plotted separately and plotted in sum to form the Green's function. The eight figures (i.e., Figs. 7–14) are plotted for different combinations of two types of Green's functions (vector and scalar), two different ε_r, and two normalized frequencies b of Mosig [1]. Here, $b = \sqrt{\varepsilon_r - 1}\,(k_0 t)$, with substrate thickness t, as mentioned at the Section IV-A. b can be used as a gauge to limit the strength of surface wave.

Each field term of a Green's function has a different attenuation rate with distance and behavior. These have been discussed in detail in the previous sections. Together, in a Green's function, there are phase differences between different terms. These show up frequently as dips and at the boundaries between field regions of near, intermediate, and far, as in Figs. 7–14. For an overall view of the behaviors of the terms and their regions, a summary is given in Table I.

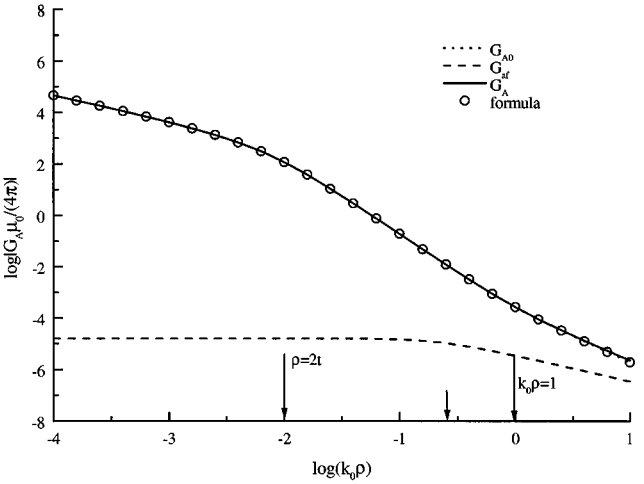

Fig. 12. Vector Green's function for $\varepsilon_r = 12.9$, $b = 0.01\pi/2$.

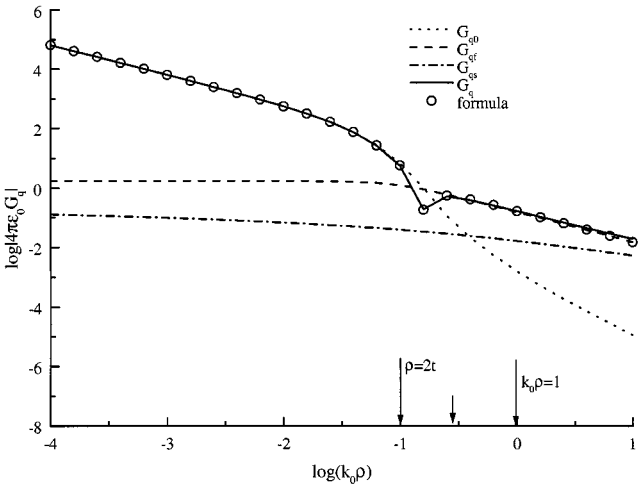

Fig. 13. Scalar Green's function for $\varepsilon_r = 12.9$, $b = 0.1\pi/2$.

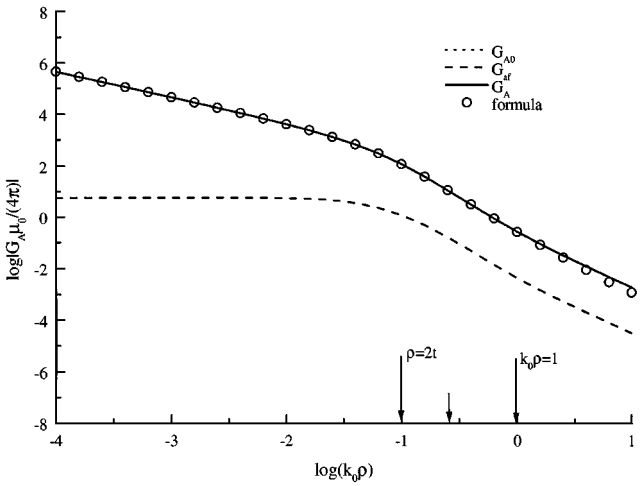

Fig. 14. Vector Green's function for $\varepsilon_r = 12.9$, $b = 0.1\pi/2$.

In Figs. 2(a) and (b), 7–14, two markers for each normalized frequency b are given. Marker 1 ($\rho = 2t$) indicates the change of the $1/\rho$ to $1/\rho^3$ dependence of the inductive quasi-dynamic field. Marker 2 ($k_0\rho = 1$) indicates the change in free space from the inductive $1/\rho^3$ dependence to the radiative $1/\rho^2$ or $1/\rho$

dependence of the quasi-dynamic field. At high frequency and high ε_r, the leaky and surface waves may flood over marker 2 toward the source, as in the scalar Green's functions of Figs. 11 and 13, and be discussed near the conclusion of Section V-A.

VII. Conclusions

The Green's functions of a microstrip substrate, both scalar and vector, are complicated in expression and behavior. This makes the gives and takes in a circuit design difficult. This paper is an effort in a series to simplify the expressions and understand the behavior. The result is three small formula sets, each for a field region of near, intermediate, and far. The formulas can be calculated by a small program, or by even a programmable calculator. The accuracy is good, from 1% to 2% error.

The formulas are simple because of the separation into parts, then the formulas of the parts are derived using different methods, whichever is the easiest and accurate. Derivation, instead of numerical fit, is normally used in this paper to ensure wide ranges of parameter values.

The advantage of the formulas lies not so much on simplicity itself, but on the ability for an engineer to observe from the simple formulas the trend in behavior in microwave circuit designs. This is useful especially with the wide ranges of the parameter values possible for a given case. A case in point is the rapid rise of surface-wave amplitude and, therefore, loss, with only a small increase in frequency, as given in (20).

This paper has only studied the most common case, which is with one layer substrate and at frequencies low enough that there is only a low-loss surface wave of the TM_0 mode propagating. Following a similar approach, other cases, such as a two-layer substrate, should be possible.

This paper has considered the vector Green's function G_A^{xx} for the horizontal x-directed current source and electric field. It does not consider G_A^{zx} for the same current source, but the vertical z-directed vector Green's function. The reason is that, in a planar circuit, there is little vertical current to interact with G_A^{zx}.

References

[1] J. R. Mosig, "Integral equation technique," in *Numerical Techniques for Microwave and Millimeter-Wave Passive Structures*, T. Itoh, Ed. New York: Wiley, 1989, pp. 155–161.

[2] P. Silvester, "TEM wave properties of microstrip transmission lines," *Proc. Inst. Elect. Eng.*, vol. 115, pp. 43–48, Jan. 1968.

[3] Y. L. Chow and I. N. El-Behery, "An approximate dynamic spatial Green's function for microstrip lines," *IEEE Trans. Microwave Theory Tech.*, vol. MTT-26, pp. 978–983, Dec. 1978.

[4] Y. L. Chow, "An approximate dynamic Green's function in three dimensions for finite length microstrip line," *IEEE Trans. Microwave Theory Tech.*, vol. MTT-28, pp. 393–397, Apr. 1980.

[5] E. Alanen and I. V. Lindell, "Exact image method for field calculation in horizontally layered medium above a conducting ground plane," *Proc. Inst. Elect. Eng.*, pt. H, vol. 133, pp. 297–304, Aug. 1986.

[6] D. G. Fang, J. J. Yang, and G. Y. Delisle, "Discrete image theory for horizontal electric dipoles in a multilayered medium," *Proc. Inst. Elect. Eng.*, pt. H, vol. 135, pp. 297–303, Oct. 1988.

[7] Y. L. Chow, J. J. Yang, D. G. Fang, and G. E. Howard, "A closed form spatial Green's function for thick microstrip substrate," *IEEE Trans. Microwave Theory Tech*, vol. 39, pp. 588–592, Mar. 1991.

[8] Y. L. Chow, J. J. Yang, and G. E. Howard, "Complex images for electrostatic field computation in multilayered media," *IEEE Trans. Microwave Theory Tech*, vol. 39, pp. 1120–1125, Mar. 1991.

[9] Y. L. Chow, N. Hojjat, S. Safavi-Naeini, and R. Faraji-Dana, "Spectral Green's functions for multilayer media in a convenient form," *Proc. Inst. Elect. Eng.*, pt. H, vol. 145, pp. 85–91, Jan. 1998.

[10] N. Hojjat, S. Safavi-Naeini, R. Faraji-Dana, and Y. L. Chow, "Fast computation of the nonsymmetrical components of the Green's function for multilayer media using complex images," *Proc. Inst. Elect. Eng.*, pt. H, vol. 145, pp. 285–288, Aug. 1998.

[11] R. Faraji-Dana and Y. L. Chow, "Accurate and effective CAD tool for the design of optimum packaging for (M)MIC's," *Proc. Inst. Elect. Eng.*, pt. H, vol. 142, pp. 81–88, Apr. 1995.

[12] I. Park, R. Mittra, and M. I. Aksun, "Numerically efficient analysis of planar microstrip configurations using closed form Green's functions," *IEEE Trans. Microwave Theory Tech.*, vol. 43, pp. 394–400, Feb. 1995.

[13] M. I. Aksun and R. Mittra, "Derivation of closed-form Green's functions for a general microstrip geometry," *IEEE Trans. Microwave Theory Tech.*, vol. 40, pp. 2055–2061, Nov. 1992.

[14] R. A. Kipp and C. H. Chan, "Complex image method for sources in bounded regions of multilayer structures," *IEEE Trans. Microwave Theory Tech.*, vol. 42, pp. 860–865, May 1994.

[15] Y. Hua and T. K. Sarkar, "Generalized pencil-of-function method for extracting poles of an EM system from its transient response," *IEEE Trans. Antennas Propagat.*, vol. 37, pp. 229–234, Feb. 1989.

[16] Y. L. Chow, A. Torabian-Esfahani, and N. Hojjat, "Simulated images for multilayer media, complex images without Prony's method," in *IEEE AP-S Int. Symp. Dig.*, Jun. 1995, pp. 818–821.

[17] A. Torabian-Esfahani and Y. L. Chow, "Simulated image method for Green's function of multilayer media," *IEEE Trans. Microwave Theory Tech.*, vol. 47, pp. 1777–1781, Sept. 1999.

[18] R. E. Collin, *Field Theory of Guided Waves*, 2nd ed. New York: IEEE Press, 1991.

Y. Leonard Chow (S'60–M'65) received the Ph.D. degree from the University of Toronto, Toronto, ON, Canada, in 1965.

From 1964 to 1966, he was with the National Radio Astronomy Observatory, Charlottesville, VA, where he designed the array configuration of the very large antenna array (VLA) of 27 25-m dishes of Soccoro NM. In 1966, he was with the University of Waterloo, Waterloo, ON, Canada, where he was involved with numerical methods and simplification of electromagnetic theory for monolithic-microwave integrated-circuit (MMIC) designs. In 1996, he joined the City University of Hong Kong, Hong Kong, where he is currently a Professor. He has been a consultant for EEsof Inc, Santa Rosa, CA, for five years. He has authored or co-authored over 250 journal and conference papers. He has five patents in the U.S. and Canada.

Wan C. Tang received the B.S. degree from Tsing Hua University, Beijing, China, in 1990, the M.S. from the Nanjing University of Science and Technology, Nanjing, China, in 1995, and is currently working toward the Ph.D. degree at the City University of Hong Kong, Hong Kong.

In 1999, he came to the City University of Hong Kong as a Research Assistant. His research interests include numerical methods and simplification of electromagnetic theory for MMIC designs.